# Design of a Continuum Mechanism That Matches the Movement of an Eight-Bar Linkage

# Xueao Liu<sup>1</sup>

School of Mechanical Engineering and Automation, Beihang University, Beijing 100191, China e-mail: liuxueao@buaa.edu.cn

# J. Michael McCarthy

Robotics and Automation Laboratory, University of California, Irvine, CA 92697 e-mail: jmmccart@uci.edu This paper presents a design methodology for mechanisms consisting of a single continuous structure, continuum mechanisms, that blends the kinematic synthesis of rigid-body mechanisms with topology optimization for compliant mechanisms. Rather than start with a generic structure that is shaped to achieve a required force-deflection task for a compliant mechanism, our approach shapes the initial structure based on the kinematic synthesis of a rigid-body mechanism for the required movement, then the structure is shaped using finite element analysis to achieve the required force-deflection relationship. The result of this approach is a continuum mechanism with the same workpiece movement as the rigid link mechanism when actuated. An example illustrates the design process to obtain an eightbar linkage that guides its workpiece in straight-line rectilinear movement. We show that the resulting continuum mechanism provides the desired rectilinear movement. A 210 mm physical model machined from Nylon-6 is shown to achieve 21.5 mm rectilinear movement with no perceived deviation from a straight-line. [DOI: 10.1115/1.4047439]

Keywords: compliant mechanisms, mechanism design, mechanism synthesis

# 1 Introduction

In this paper, we present a design methodology for mechanisms formed as a single continuous structure that deforms to provide useful mechanical movement. Inspired by the continuum robots used in medical [1], firefighting [2], and other [3] applications, we refer to these devices as continuum mechanisms. These mechanisms are manufactured as a single part so there is no assembly and components do not slide relative to each other so there is no lubrication [4–6]. The goal of this paper is to merge techniques for kinematic synthesis of rigid link mechanisms with those for the design of compliant mechanisms [7,8] in order to obtain an effective design methodology for continuum mechanisms.

An important design methodology for compliant mechanisms is known as topology optimization, in which a structure of truss or beam elements is modified to achieve a design goal that combines movement and distributed stresses [9]. Cao et al. [7] modify topology optimization in order to design rigid link mechanisms, a process they call module optimization. Valentini and Pennestri [8] present an alternate approach to combining rigid link and compliant link synthesis that uses a mechanical representation of compliant link movement, which can be formulated using the equations of kinematic synthesis.

Our approach arises from viewing topology optimization as consisting of two phases: a first phase that transforms a generic domain into a structure for the device and a second phase that modifies the dimensions of the elements of this structure to obtain the required force-deflection relationship for the device. Instead of modifying a network of truss or beam elements to find the structure of the device, as the first phase, we identify structures that match rigid link mechanisms that achieve the required movement. The second phase continues as before with the dimensions of these structures modified and evaluated using finite element analysis (FEA) to

<sup>1</sup>Corresponding author.

Contributed by the Mechanisms and Robotics Committee of ASME for publication in the JOURNAL OF MECHANISMS AND ROBOTICS. Manuscript received November 26, 2019; final manuscript received May 19, 2020; published online July 17, 2020. Assoc. Editor: Stephen Canfield.

obtain the required force-deflection relationship for the continuum mechanism.

The use of rigid-body synthesis has the advantage that many design candidates can be generated and evaluated to identify those in which the links move as required without any overlap. A reference position of the model linkage is used to define a structure with specific material properties that are to move under a given applied load. Special regions for deformation are introduced around the joints of the kinematic model defined by parameterized boundary curves. Finite element analysis is then used to adjust the parameters for each of these regions to both provide the desired movement and reduce the Von Mises stresses in the entire structure. We present an example of this design methodology and obtain a 210 mm × 120 mm physical model that provides 21.5 mm of rectilinear movement with a deviation from a straight-line less than is visually detectable.

### 2 Literature Review

Topology optimization generates both a distribution of structural elements for the compliant mechanism as well as the dimensions of these elements [9]. Cao et al. [10] identify 12 different tasks and objective functions for the design of compliant mechanisms using topology optimization. A survey of design techniques for rigid link mechanisms is provided by McCarthy and Soh [11]. The application of kinematic synthesis to the design of a wide range of eightbar linkages is presented by Sonawale and McCarthy [12,13].

Models of compliant mechanisms can be constructed using rigid bodies and spring joints, see, for example, Su [14], who models the tip movement of an elastic beam under large deflection using three rigid links connected by three springs. It is possible to apply kinematic synthesis of rigid links connected by spring joints as described in Su and McCarthy [15]. However, Valentini and Pennestri [8] describe the need to move beyond this approach.

On the surface, our focus on special regions of deformation is similar to the design of flexures described in the books by Howell [4] and Lobontiu [16], also see Linß and Milojevic [17]. However, an important distinction is that our entire structure is

compliant and the relative compliance of various regions is controlled by the parameters that define the boundaries of the regions of deformation. In addition, we seek designs that limit the Von Mises stresses in the entire mechanism.

Our example focusses on continuum mechanisms that provide pure rectilinear movement because they have practical applications in the design of suspensions to the support linear movement [18–21]. The models for these continuum mechanisms are rigid link mechanisms that guide a workpiece along rectilinear movement, which were studied by Kempe [22] and more recently by Hao et al. [20]. These mechanisms are complex and include overlapping links with large relative joint rotations that do not yield practical continuum mechanisms [16,23,24]. There is, however, an advantage to linkages that are more complex than a four-bar linkage, because they can distribute movement over more joints, 10 joints in the case of an eight-bar linkage [12]. Therefore, our goal is to find eight-bar linkages with non-overlapping links that provide the required movement, which we use as model structures for our continuum mechanism synthesis process.

# 3 The Design Step

In order to design a continuum mechanism, we begin with the design of a conventional linkage that achieves the desired movement; in this case, the mechanism is to guide the workpiece in a rectilinear movement, such that the supporting links do not overlap during the movement. Once this conventional mechanism is achieved in a schematic form, see Fig. 1, we convert the mechanism into a structure with special regions of deformation located at each of the joints. Geometric operations are used to widen each bar and smooth its attachment to the flexure region. Finally, the parameters that define the flexure regions are adjusted using finite element analysis in order to obtain dimensions that yield the desired movement of the workpiece.

# 4 Design of Rigid Eight-Bar Linkages

In order to design an eight-bar linkage with ideal revolute joints that has one degree-of-freedom, we select two RRR (R denotes a revolute joint) chains that move its end-effectors through the required five task positions which are on a straight line. The inverse kinematics of a RRR chain can define the positions of each of its links in each configuration, thus, a six-R loop chain can be obtained by a combination of two RRR chains. Furthermore, based on the six-R chain, we compute two RR constraints that maintain the required relative positions of the links. The resuls is an eight-bar linkages [12,25,26]. With this method, we can obtain 32 eight-bar linkages. At last, we select one which has no links overlap and small relative joint rotations.

**4.1** Inverse Kinematics of a RRR Chain. As shown in Fig. 2(a), let homogeneous transforms  $[T_i]$ , i=1, ..., 5 denote the five task positions which are on the same straight line, the positions of each link frame can be denoted as  $[A_j]$ , j=1, ..., 3. Let [E] denote the transformation matrix that maps the base of the RRR chain to ground frame F and [H] denote the transformation matrix of end-effector in the last link  $A_3$  frame. So, the kinematics equations of a RRR chain can be given by

$$[T_i] = [E] \cdot [A_1(\theta_{1i})] \cdot [A_2(\theta_{2i}, a_1)] \cdot [A_3(\theta_{3i}, a_2)] \cdot [H]$$
 (1)

where  $\theta_{1i}$ ,  $\theta_{2i}$ ,  $\theta_{3i}$ , i = 1, ..., 5 denote the relative joint rotation angles at the five task positions respectively, and link lengths  $a_1$ ,  $a_2$  are constants and specified by the designer.

For the convenience of calculations, instead of specifying [E], [H],  $a_1$ , and  $a_2$ , we give the locations of  $C_1$ ,  $C_2$ , and  $C_3$  joints. Then, we can solve two inverse kinematics equations of the RRR chain, where the two RRR chains pass through the same five task

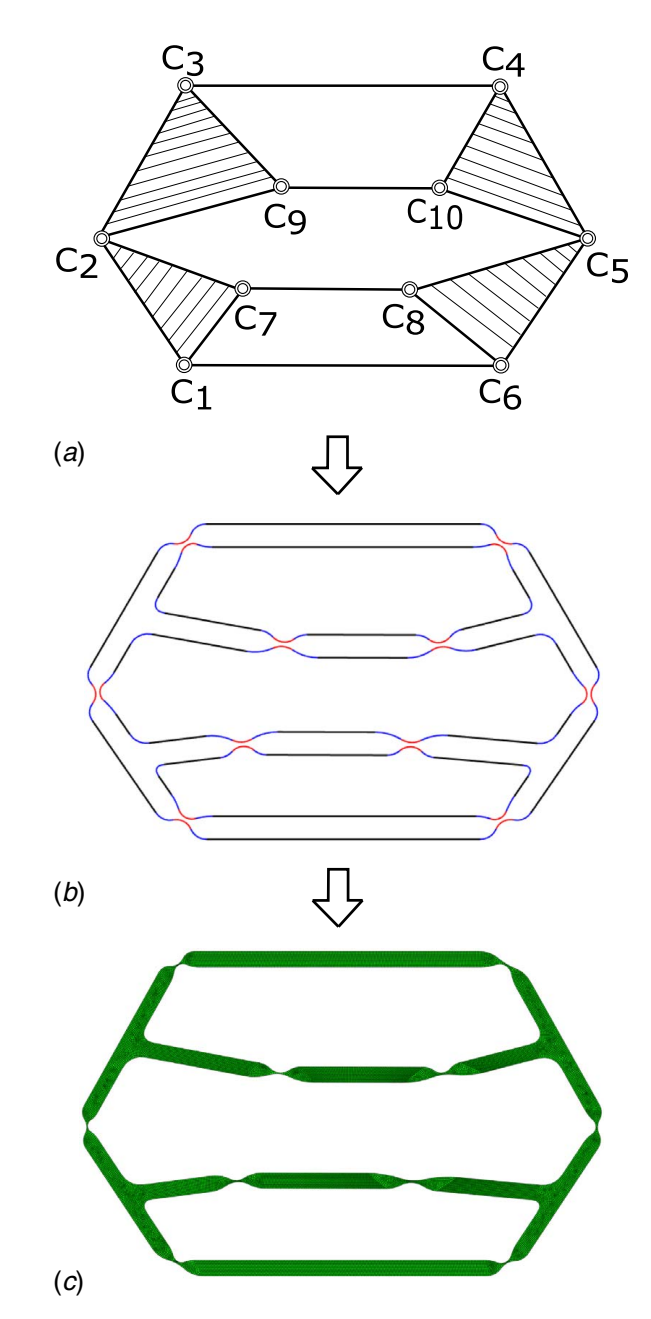


Fig. 1 The design step: (a) design of a rigid eight-bar linkage for rectilinear movement, (b) converting the rigid linkage into a structure with special regions of deformation located at each of the joints by geometric operations, and (c) adjusting the geometry of these regions using finite element analysis to obtain a continuum mechanism

positions, to obtain the location of each joint to construct a six-R loop chain, see Fig. 2.

**4.2 Synthesis of a RR Constraint.** As shown in Fig. 3, let  $W_i$  and  $G_i$ , i = 1, ..., 5 denote the five sets of points that on the different two moving links of the six-R chain at the five task positions configurations, and  $[B_i]$  and  $[D_i]$  are the  $3 \times 3$  homogeneous transforms of the different two moving links, respectively. Let  $\mathbf{w}$  and  $\mathbf{g}$  denote the coordinates of the corresponding points of  $\mathbf{W_i}$  and  $\mathbf{G_i}$  which are measured in the  $[B_i]$  and  $[D_i]$  local frame, respectively. Thus, we can obtain

$$\mathbf{W_i} = [B_i]\mathbf{w} \quad \text{and} \quad \mathbf{G_i} = [D_i]\mathbf{g}$$
 (2)

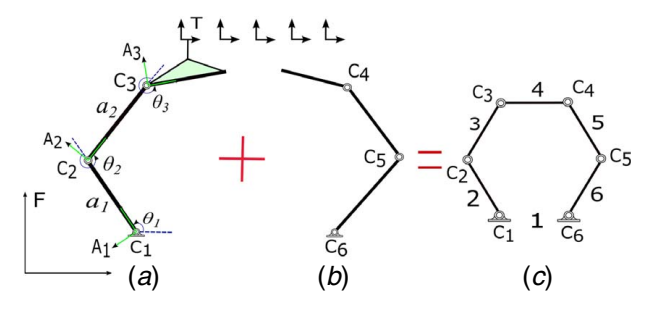


Fig. 2 Giving the positions of joints  $C_i$ ,  $i=1,\ldots,6$  to construct two RRR chains through the same five task positions to form a 6R chain

The synthesis equations are obtained by constraining the length of link  $W_1G_1$  to be a constant R,

$$([B_i][B_1]^{-1}\mathbf{W}_1 - [D_i][D_1]^{-1}\mathbf{G}_1).([B_i][B_1]^{-1}\mathbf{W}_1$$

$$-[D_i][D_1]^{-1}\mathbf{G}_1) = R^2, \quad i = 1, \dots, 5$$
(3)

Then, we can obtain the locations of points  $W_1$  and  $G_1$  by solving Eq. (3). Here,  $[B_i]$  and  $[D_i]$ ,  $i=1,\ldots,5$  are the positions of two moving links of the six-R chain when it passes through the five task positions, respectively. Then, two RR constraints are added to the six-R chain to result in an eight-bar linkage with one degree-of-freedom. There are five moving links in our 6R chain, and any two of them can be constrained by the RR constraint. With the method of permutation and combination and eliminating the cases that are invalid, we can obtain 32 valid eight-bar linkages, see Fig. 4. In addition, each of the linkages has 10 revolute joints.

**4.3 Numerical Example.** In this section, we give five task positions (0 mm, 0 mm), (25 mm, 0 mm), (50 mm, 0 mm), (75 mm, 0 mm), (100 mm, 0 mm) that on a straight line as an example to calculate a desired eight-bar linkage, and all orientation angles of these positions are 0 radians. According to the fabrication of compliant mechanisms, our goal is to design an eight-bar linkage that avoids overlap and large relative joint rotations. It means that to find an eight-bar linkage that all links have no overlap each other and each joint has no large rotation angle. Here, due to the locations

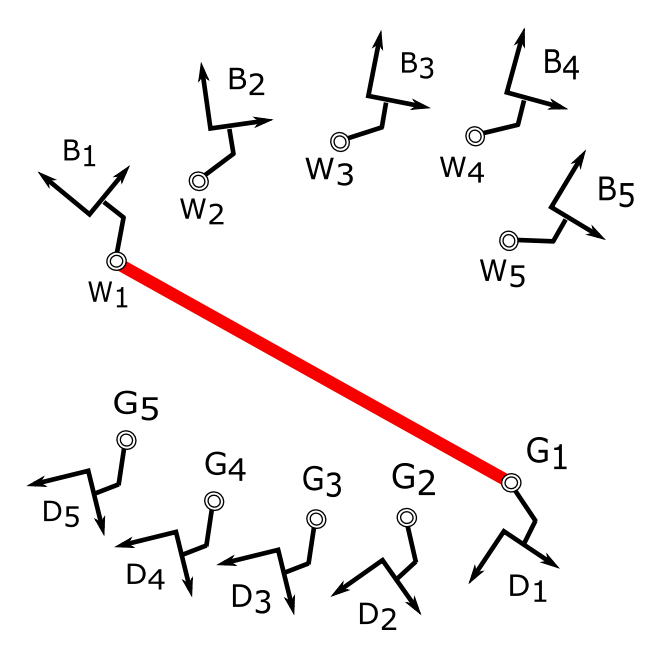


Fig. 3 A series of positions W<sub>i</sub> and G<sub>i</sub> of RR constraint

of joints  $C_i$ , i = 1, ..., 6 are given by the designer, the Eq. (3) may have no solution when these initial values are inappropriate. A tolerance is set around the initial values and randomly selected values allow the calculation of more solutions. In addition, we select joints locations for the 6R closed chain that are symmetric to the Y-axis. For each solution, we verify that it has no defects. One of these solutions is shown in Fig. 5, and the coordinates of each joint are listed in Table 1.

# 5 Geometric Design of the Continuum Mechanism

In this section, we give a process of transforming the above rigid eight-bar linkage into a continuous structure by a series of geometric transformations. We aim to design a fully compliant mechanism, which can achieve the same workpiece movement as the rigid mechanism when actuated. Therefore, we let the thinnest part of the flexure regions be located at the same location of ideal revolute joints, this helps to make the deformation center of the flexure regions be coincide with the revolute joint locations. In this paper, each geometry of flexure regions is determined by three independent parameters, and we can control the movement performance of the continuum mechanism by adjusting these three parameter values.

**5.1 Widening Each Bar.** In this step, bars are widened by a specified width to produce realistic links to hold the continuum mechanism. As shown in Fig. 5, the rigid eight-bar linkage consists of four triangular members and four linear members. If we use the joint points to describe the above members, four triangular members are denoted as  $C_1C_2C_7$ ,  $C_2C_3C_9$ ,  $C_4C_5C_{10}$ ,  $C_5C_6C_8$ , and four linear members are  $C_1C_6$ ,  $C_3C_4$ ,  $C_7C_8$ ,  $C_9C_{10}$ . To make the geometry of the continuum mechanism easier to design, we convert all the triangular members into linear members. Here, we introduce points  $C_{11}$ ,  $C_{12}$ ,  $C_{13}$ , and  $C_{14}$  as the midpoints of lines  $C_1C_2$ ,  $C_2C_3$ ,  $C_4C_5$ , and  $C_5C_6$ , respectively. Then, we connect point  $C_{11}$  to  $C_7$ ,  $C_{12}$  to  $C_9$ ,  $C_{13}$  to  $C_{10}$ , and  $C_{14}$  to  $C_8$  to form a new geometry, as shown in Fig. 6. Notice that points  $C_{11}$ ,  $C_{12}$ ,  $C_{13}$ , and  $C_{14}$  are not the locations of revolute joint.

As shown in Fig. 7, one of bars  $C_m C_n$  is selected to show our widening method, where m, n = 1, ..., 14 and  $m \neq n$ . Four points are generated when the bar  $C_m C_n$  is widened, which are denoted as  $C_{mn}^1$ ,  $C_{mn}^2$ ,  $C_{mn}^3$  and  $C_{mn}^4$ . To calculate the locations of these four new points, we introduce a unit direction vector, which is as follows,

$$\overrightarrow{C_m}\overrightarrow{C_n} = \frac{\overrightarrow{C_n} - \overrightarrow{C_m}}{\|\overrightarrow{C_n} - \overrightarrow{C_m}\|} \tag{4}$$

where  $\overrightarrow{C_m}$ ,  $\overrightarrow{C_n}$  denote the position vectors of  $C_m$  and  $C_n$  relative to ground frame origin, respectively, and  $\overrightarrow{C_mC_n}$  denotes the unit vector of  $C_n$  relative to  $C_m$ .

Then, we can obtain the position vectors of  $C_{mn}^1$ ,  $C_{mn}^2$ ,  $C_{mn}^3$ , and  $C_{mn}^4$  relative to ground frame origin, which are as follows:

$$\vec{C}_{mn}^{1} = \vec{C}_{m} + r_{mn}h \cdot \frac{\vec{\eta} \times \overrightarrow{C_{m}C_{n}}}{\|\vec{\eta} \times \overrightarrow{C_{m}C_{n}}\|}$$

$$\vec{C}_{mn}^{2} = \vec{C}_{m} - (1 - r_{mn})h \cdot \frac{\vec{\eta} \times \overrightarrow{C_{m}C_{n}}}{\|\vec{\eta} \times \overrightarrow{C_{m}C_{n}}\|}$$

$$\vec{C}_{mn}^{3} = \vec{C}_{n} + r_{mn}h \cdot \frac{\vec{\eta} \times \overrightarrow{C_{m}C_{n}}}{\|\vec{\eta} \times \overrightarrow{C_{m}C_{n}}\|}$$

$$\vec{C}_{mn}^{4} = \vec{C}_{n} - (1 - r_{mn})h \cdot \frac{\vec{\eta} \times \overrightarrow{C_{m}C_{n}}}{\|\vec{\eta} \times \overrightarrow{C_{m}C_{n}}\|}$$

$$(5)$$

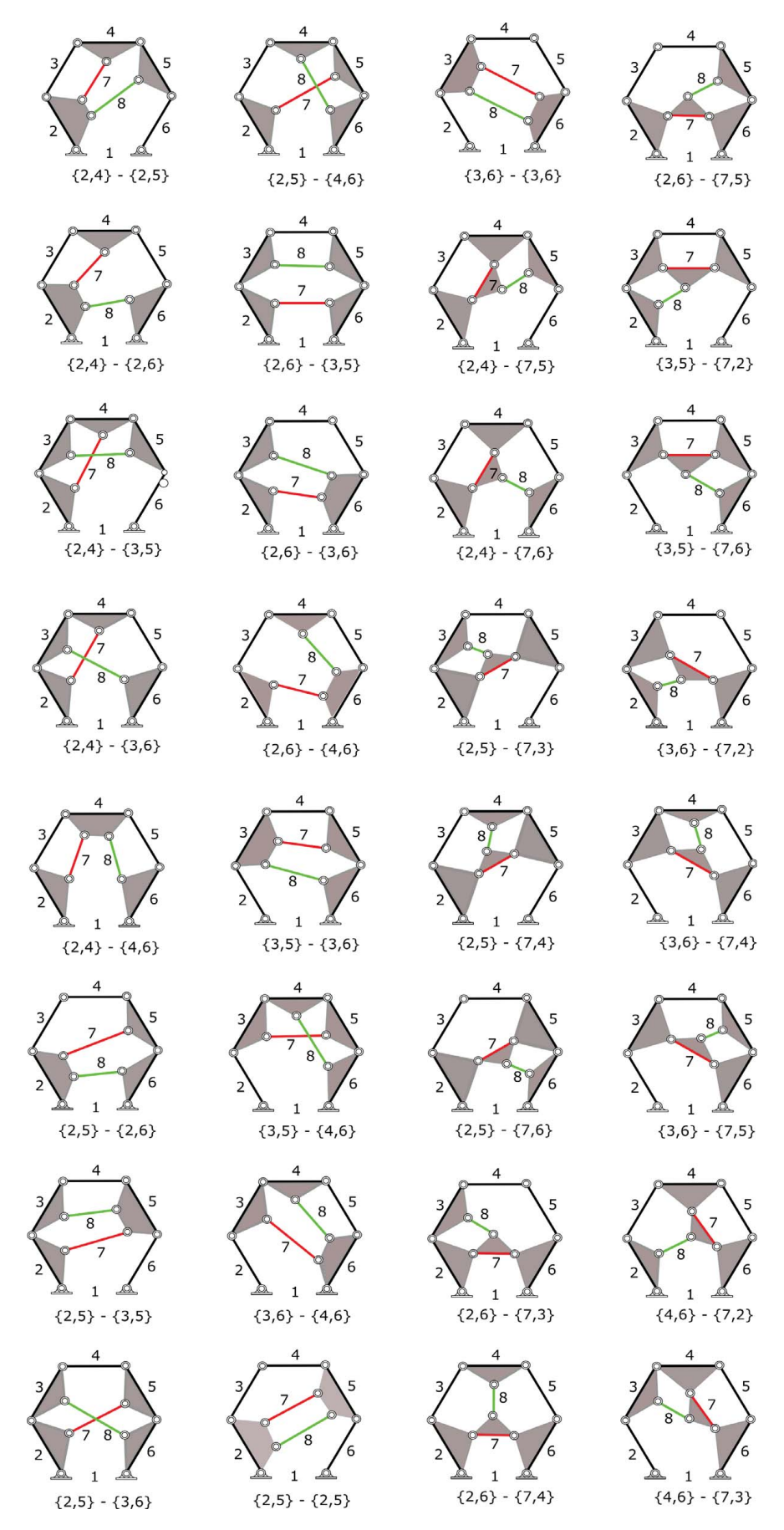


Fig. 4 Adding two RR constraints to a 6R chain to generate 32 eight-bar linkages with one degree-of-freedom

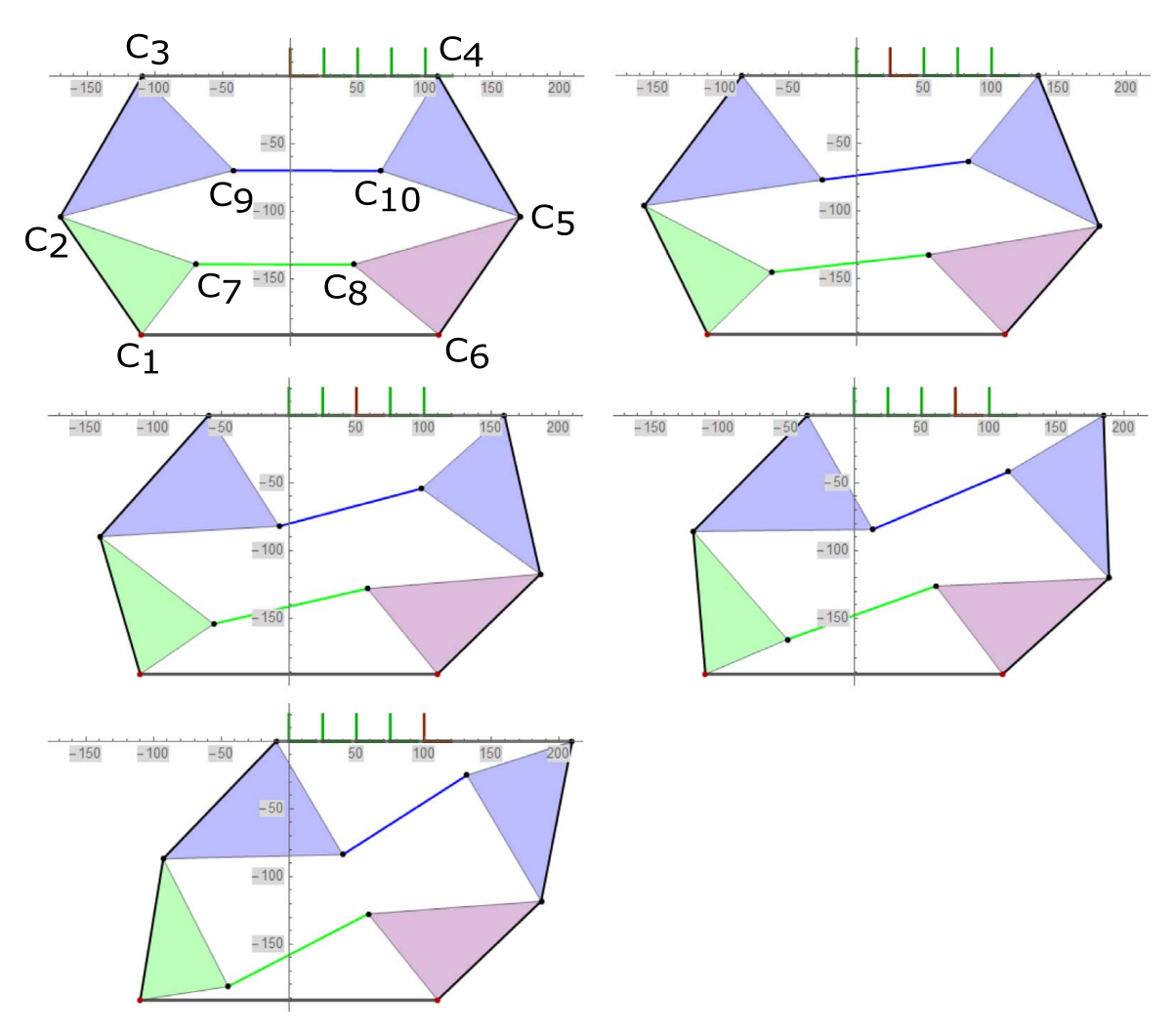


Fig. 5 The designed eight-bar linkage with 10 revolute joints and non-overlap moves through the five task positions, respectively

where  $\vec{\eta} = (0, 0, 1)$  and denotes the unit vector which is perpendicular to the paper,  $r_{mn}$  denotes the widening ratio, h denotes the widening width. After  $C_m C_n$  is widened,  $C_{mn}^1$ ,  $C_{mn}^2$ ,  $C_{mn}^3$ , and  $C_{mn}^4$  constitute two new sides, which are denoted as  $C_{mn}^1 C_{mn}^3$  and  $C_{mn}^2 C_{mn}^4$ , respectively. For convenience, we define  $C_{mn}^1 C_{mn}^3$  as the outside and  $C_{mn}^2 C_{mn}^4$  as the inside.

5.1.1 Widening Constraint. In order to make the thinnest part of flexure region can be designed at the location of revolute joint in the following sections, a constraint is introduced when widening

Table 1 The locations of the 10 revolute joints of the designed eight-bar linkage

Joint	Location (mm)		
$C_1$	(-109.91, -191.43)		
$C_2$	(-169.99, -104.86)		
$C_3$	(-109.44, 0)		
$C_4$	(109.44, 0)		
$C_5$	(169.99, -104.08)		
$C_6$	(109.91, -191.43)		
$C_7$	(-69.94, -139.16)		
$C_8$	(46.78, -139.45)		
$C_9$	(-41.71, -69.76)		
$C_{10}$	(67.26, -70.04)		

these bars. The constraint is that the widening ratios of two adjacent bars that are connected by a revolute joint need to be equal. Figure 8 displays two different widening cases of two adjacent bars, there are two adjacent bars connected by a revolute joint, which are denoted as  $C_m C_n$  and  $C_q C_m$ . In addition, we use  $r_{mn}$  to denote the widening ratio of  $C_m C_n$  and use  $r_{qm}$  to denote the widening ratio of  $C_q C_m$ .  $P_m^1$  and  $P_m^2$  denote the intersection points of the outside and the inside, respectively. When  $r_{mn} = r_{qm}$ , line  $P_m^1 P_m^2$  can pass through  $C_m$ , as

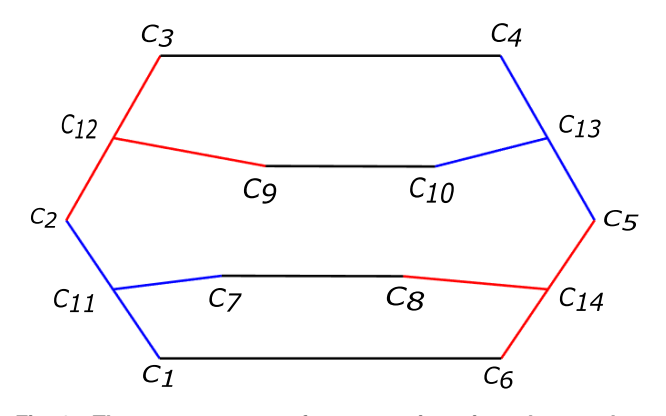


Fig. 6 The new geometry after converting triangular members into linear members

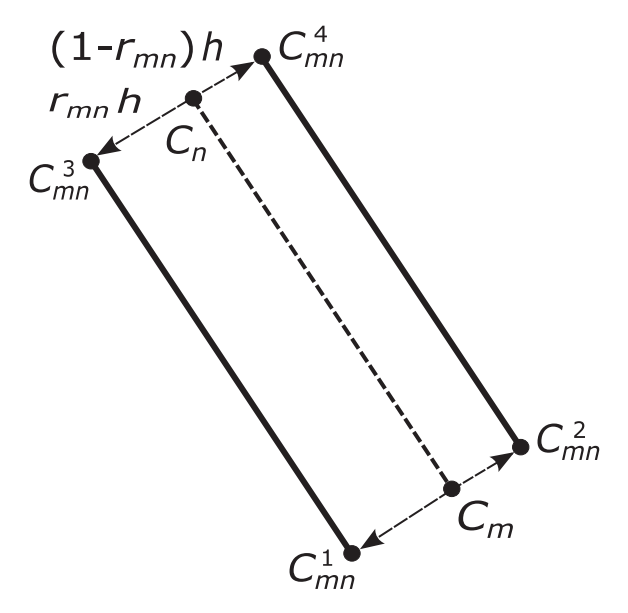
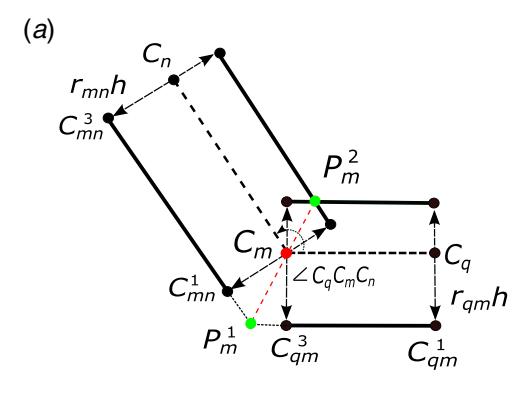


Fig. 7 Four points are generated by widening bar  $C_mC_n$  with the ratio  $r_{mn}$  and width h

shown in Fig. 8(*a*). Otherwise, line  $P_m^1 P_m^2$  can not pass through  $C_m$ . This example can clearly explain the reason for adding constraints.

5.1.2 Widening Ratio. As shown in Fig. 9, we define  $\angle C_q C_m C_n$  as the included angle between two adjacent bars, and the range of  $\angle C_q C_m C_n$  is from 0 to  $\pi$ . The widening ratios of two adjacent bars are determined by the angle, so we give the following rule. When the angle  $\angle C_q C_m C_n$  is equal to or less than  $\pi/2$ , the two widening ratios  $r_{mn} = r_{qm} = 1$ , see Figs. 9(a) and 9(b). When the angle is equal to  $\pi$ ,  $r_{mn} = r_{qm} = 0.5$ , see Fig. 9(c). When the angle



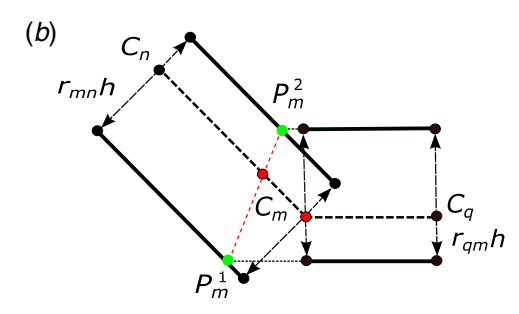


Fig. 8 (a) The case of intersection of widening bar  $C_mC_n$  and  $C_qC_m$  with  $r_{mn}=r_{qm}$  and (b) the case of intersection of widening bar  $C_mC_n$  and  $C_qC_m$  with  $r_{mn}\neq r_{qm}$ 

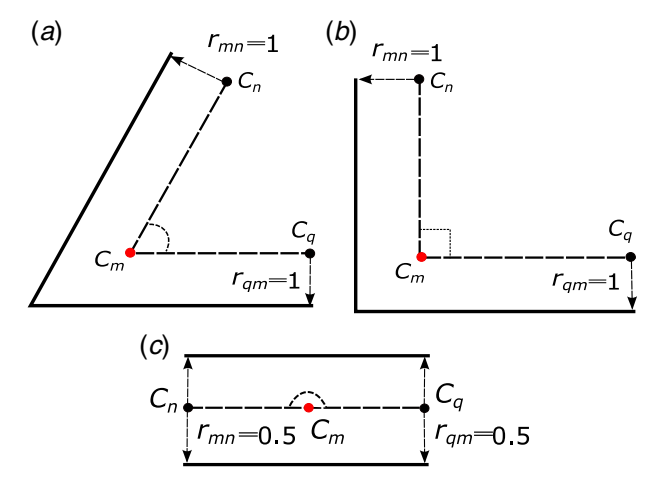


Fig. 9 (a) When the angle  $\angle C_q C_m C_n$  is less than  $\pi/2$ , the two widening ratios  $r_{mn} = r_{qm} = 1$ , (b) when  $\angle C_q C_m C_n$  is equal to  $\pi/2$ ,  $r_{mn} = r_{qm} = 1$ , and (c) when  $\angle C_q C_m C_n$  is equal to  $\pi$ ,  $r_{mn} = r_{qm} = 0.5$ 

is between  $\pi/2$  and  $\pi$ , the widening ratios are a linear function of this angle. We can easily get the linear function based on the values at  $\pi/2$  and  $\pi$ . Then, we can obtain the widening ratio equation

$$r_{mn} = r_{qm} = \begin{cases} 1 & \angle C_{q} C_{m} C_{n} \le \pi/2 \\ 1 - \frac{\angle C_{q} C_{m} C_{n} - \pi/2}{\pi} & \angle C_{q} C_{m} C_{n} > \pi/2 \end{cases}$$
(6)

Since  $C_{11}$ ,  $C_{12}$ ,  $C_{13}$ , and  $C_{14}$  are not the locations of revolute joints, see Fig. 6, these bars can be divided into three groups, and bars in each group are adjacent each other. The first group is made up of  $C_1C_2$ ,  $C_2C_3$ ,  $C_3C_4$ ,  $C_4C_5$ ,  $C_5C_6$ ,  $C_6C_1$ , the second group includes  $C_{11}C_7$ ,  $C_7C_8$ ,  $C_8C_{14}$ , and the third group consists of  $C_{12}C_9$ ,  $C_9C_{10}$ ,  $C_{10}C_{13}$ . According to the widening constraint, all the bars in the group should have the same ratio. Here, we take the smallest angle in each group to calculate by using Eq. (6) as the final widening ratio. Figure 10 shows the geometry after widening each bar.

5.2 Geometric Design of Flexure Region. The geometry of flexure region affects the movement performance of the continuum mechanism directly. In order to match the movement of the rigid eight-bar linkage, we propose to construct the geometry of flexure region by combining the circular sections and Bezier curves. In addition, let the geometry of flexure region be an axial symmetric figure. This helps to make flexure region deformation center be at the same location as the revolute joint. In addition, each geometry

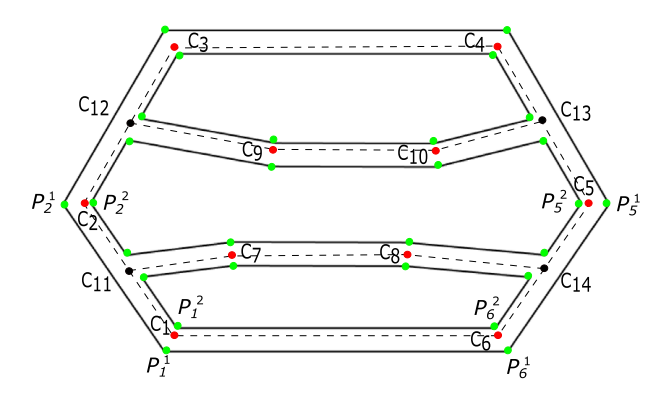


Fig. 10 The geometry after widening each bar

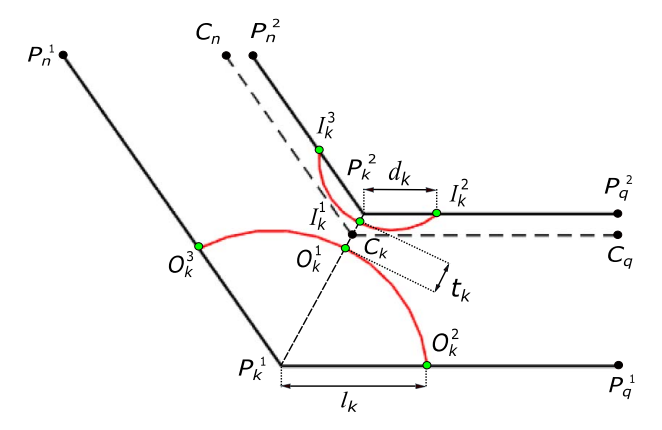


Fig. 11 Six points are determined by three parameters to construct two circular sections in the location of revolute joint  $C_k$ 

of flexure region is parameterized by three parameters, that will make it easier to control the deformation movement and distribute stress uniformly.

5.2.1 Circular Section. It is generally known that a circular arc can be determined by three points that are not collinear. Here, we construct two circular arcs by using six points. And these six points are determined by three parameters. Figure 11 displays the case of revolute joint  $C_k$ ,  $k=1,\ldots,10$  with two widened bars  $C_kC_n$  and  $C_qC_k$ . For the convenience of description, we define the circular arc which is constructed by points  $O_k^1$ ,  $O_k^2$ ,  $O_k^3$  as outside arc and the circular arc which is constructed by points  $I_k^1$ ,  $I_k^2$ ,  $I_k^3$  as inside arc, respectively. We introduce the first parameter  $t_k$  to determine the locations of points  $O_k^1$  and  $I_k^1$ , let point  $C_k$  be the midpoint of points  $O_k^1$  and  $I_k^1$ ; besides, these two points should be on line  $P_k^1P_k^2$ . This is the key to make the deformation center of flexure region be at the same location as revolute joint. The locations of points  $O_k^1$  and  $I_k^1$  can be calculated by

$$\vec{O}_k^1 = \vec{C}_k - \frac{1}{2}t_k \cdot \overrightarrow{P_k^1 P_k^2}$$

$$\vec{I}_k^1 = \vec{C}_k + \frac{1}{2}t_k \cdot \overrightarrow{P_k^1 P_k^2}$$
(7)

where  $\overrightarrow{P_k^1P_k^2}$  is the unit direction vector from  $P_k^1$  to  $P_k^2$ .

We introduce the second parameter  $I_k$  to determine points  $O_k^2$  and  $O_k^3$ , and the third parameter  $d_k$  to determine points  $I_k^2$  and  $I_k^3$ . Let the distances between  $O_k^2$  and  $O_k^3$  to  $P_k^1$  are equal, so do points  $I_k^2$  and  $I_k^3$ . Then, we obtain,

$$\vec{O}_k^2 = \vec{P}_k^1 - l_k \cdot \overrightarrow{P_q^1 P_k^1}$$

$$\vec{O}_k^3 = \vec{P}_k^1 + l_k \cdot \overrightarrow{P_k^1 P_n^1}$$
(8)

and

$$\vec{I}_k^2 = \vec{P}_k^2 - d_k \cdot \overrightarrow{P_q^2 P_k^2}$$

$$\vec{I}_k^3 = \vec{P}_k^2 + d_k \cdot \overrightarrow{P_k^2 P_n^2}$$
(9)

Therefore, we can construct the outside arc with the three points  $O_k^1,\,O_k^2,\,O_k^3$  by

$$(x_{O_k^0} - x_{O_k^1})^2 + (y_{O_k^0} - y_{O_k^1})^2 = r_O^2$$

$$(x_{O_k^0} - x_{O_k^2})^2 + (y_{O_k^0} - y_{O_k^2})^2 = r_O^2$$

$$(x_{O_k^0} - x_{O_k^3})^2 + (y_{O_k^0} - y_{O_k^3})^2 = r_O^2$$
(10)

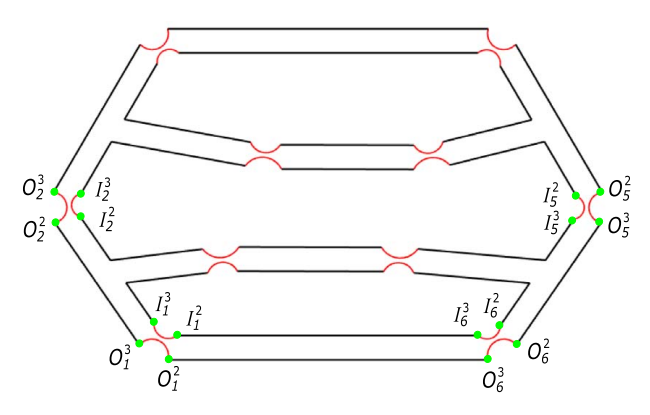


Fig. 12 The geometry after constructing arcs for each revolute ioint

where  $O_k^0$  and  $r_O$  denote the center and radius of the outside arc. Likewise, the inside arc can be constructed by the three points  $I_k^1$ ,  $I_k^2$ ,  $I_k^3$ . Figure 12 shows the geometry that all circular arcs are constructed, and each shape of regions can be controlled by the corresponding three parameters.

5.2.2 The Ranges of the Three Parameters. To ensure that the flexure region can be constructed without interference with each other, the values of  $t_k$ ,  $l_k$ , and  $d_k$  should be within reasonable ranges. It is clear that  $t_k$  should be much smaller than the width of bar. Here, we let the maximum and minimum of  $t_k$  be denoted as  $(t_k)_{\max}$  and  $(t_k)_{\min}$ , respectively. Due to the limitation of bar width, the cases when  $l_k$  takes maximum and minimum are shown in Fig. 13. The case of minimum value occurs when outside arc and line  $P_k^1 P_q^1$  are tangent. According to this constraint, we can derive the minimum value of  $l_k$ ,

$$(l_k)_{\min} = \frac{\|\overrightarrow{O_k^1 P_k^1}\| \cos(\angle C_q C_k C_n / 2)}{1 + \sin(\angle C_q C_k C_n / 2)}$$
(11)

where  $\|\overrightarrow{O_k^1} \overrightarrow{P_k^1}\|$  denotes the length of line  $O_k^1 P_k^1$ .

In addition, to form an outside arc, the maximum of  $l_k$  should be smaller than the distance between  $P_k^1$  and  $O_k^4$ , where  $O_k^4$  is the intersection point of line  $O_k^1O_k^4$  and line  $P_k^1P_q^1$ . This case occurs when line  $O_k^1O_k^4$  is perpendicular to line  $O_k^0O_k^1$ . So, the maximum value of

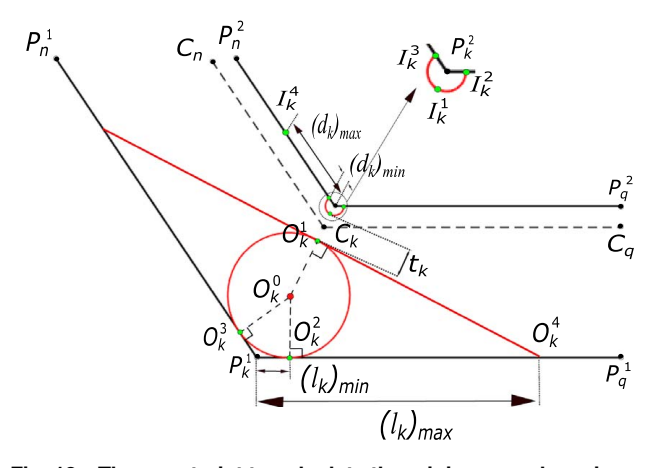


Fig. 13 The constraint to calculate the minimum and maximum of parameters  $I_k$  and  $d_k$ 

parameter  $l_k$  can be calculated by

$$(l_k)_{\text{max}} = \frac{\|\overrightarrow{O_k^1} \overrightarrow{P_k^1}\|}{\cos(\angle C_a C_k C_n / 2)}$$
(12)

For parameter  $d_k$ , there is no geometric constraint to limit its value range except for interfering with other lines. Here, we specify that its minimum value is equal to  $\|I_k^1 P_k^2\|$ , and the maximum value is equal to one half of  $\|P_a^2 P_k^2\|$ .

5.2.3 Smoothing the Flexure Region. To decrease the stress concentration of the flexure region when the mechanism is deformed, we use the Bezier curve to smooth the flexure regions. Our use is the cubic trigonometric Bezier curve which has four points to control its shape easily. The equation of cubic trigonometric Bezier curve is as follows:

$$Bezier(\theta, \lambda) = (1 - \sin \theta)^2 \vec{P} 1 + \sin \theta (1 - \sin \theta)$$

$$\times (2 + \lambda (1 - \sin \theta)) \vec{P} 2 + \cos \theta (1 - \cos \theta)$$

$$\times (2 + \lambda (1 - \cos \theta)) \vec{P} 3 + (1 - \cos \theta)^2$$

$$\times (1 - \lambda \cos \theta) \vec{P} 4, \quad 0 \le \theta \le \pi/2$$

$$(13)$$

where P1, P2, P3, P4 are the four control points and  $\theta$  is the parameter to determine the location of points on the curve.  $\lambda$  is the shape parameter, and it is equal to 1 here. Figure 14 displays an example

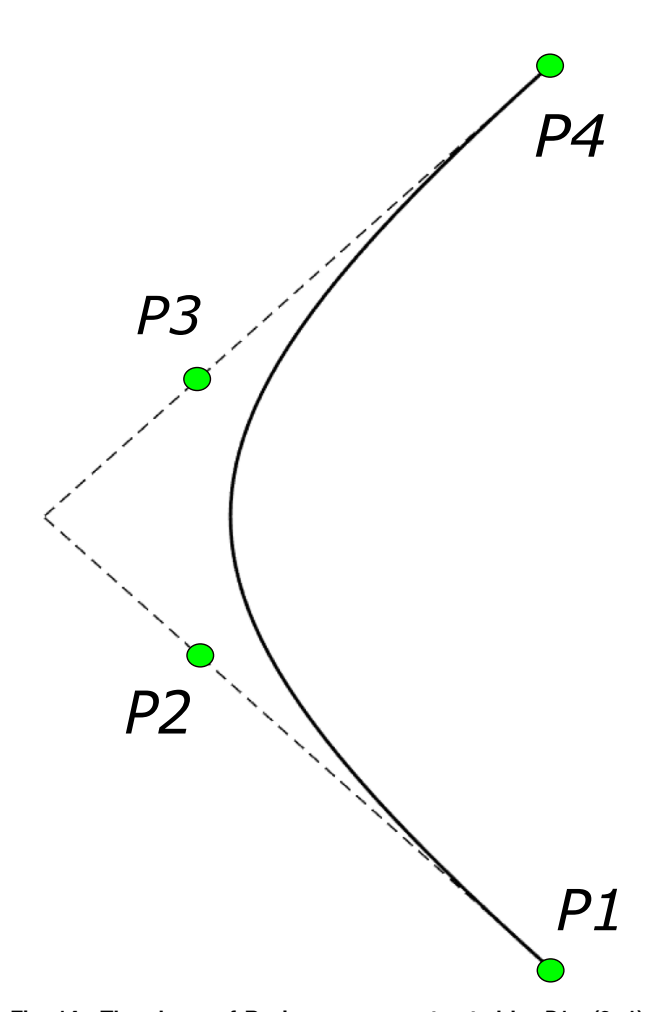


Fig. 14 The shape of Bezier curve constructed by P1=(2, 1), P2=(1, 2), P3=(1, 3), P4=(2, 4), and  $\lambda=1$ 

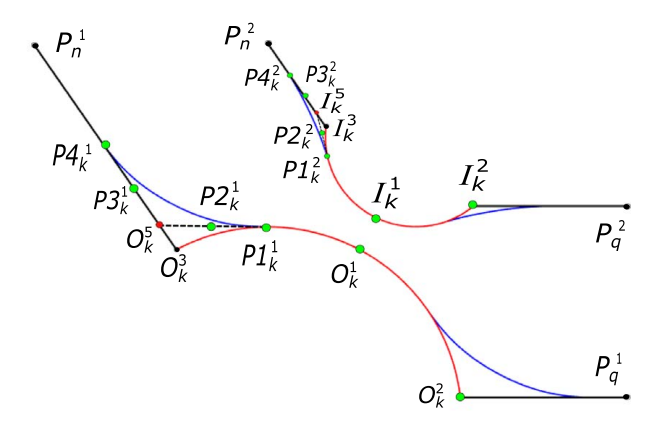


Fig. 15 The four points are determined to construct Bezier curves for outside arc and inside arc, respectively

of the Bezier curve shape with P1 = (2, 1), P2 = (1, 2), P3 = (1, 3), and P4 = (2, 4). The most important property of Bezier curve is that the unit derivative vectors at points P1 and P4 are matched to unit vectors  $\overrightarrow{P1P2}$  and  $\overrightarrow{P3P4}$ , respectively.

Accordingly, we need to determine the locations of these four points to construct Bezier curves for each of flexure regions. As shown in Fig. 15, for outside arc, the first point  $P1_k^1$  must be on the arc and the fourth points  $P1_k^4$  must be on line  $O_k^3 P_n^1$  because of the Bezier curve's property. Here, we let point  $P1_k^1$  be the midpoint of points  $O_k^1$  and  $O_k^3$ . Then, plot the line  $P1_k^1 O_k^5$  that passes through point  $P1_k^1$  and intersects line  $O_k^3 P_n^1$  at point  $O_k^5$  with the constraint of making unit direction vector  $P1_k^1 O_k^5$  be matched to the unit derivative vectors of points  $P1_k^1$  on the outside arc. Then, let point  $P2_k^1$  be the midpoint of points  $P1_k^1$  and  $O_k^5$ . To determine the locations of point  $P3_k^1$  and  $P4_k^1$ , we let  $P2_k^1 O_k^5 = |O_k^5 P3_k^1| = |P3_k^1 P4_k^1|$ .

We use the same strategy to construct the Bezier curve for inside arc, the only difference is to specify the location of the first point  $P1_k^2$ . Because the curvature of inside arc is greater than outside arc's and to avoid point  $P4_k^2$  exceeding point  $P_n^2$  and interfering with other lines, we let point  $P1_k^2$  be at the location of one third of arc  $I_k^1I_k^3$  and close to point  $I_k^3$ .

We can obtain the complete shape of the flexure region according to its symmetry. Figure 16 shows the final geometry of the continuum mechanism.

# **6** Finite Element Analysis

In the previous two sections, we constructed a parameterized geometric continuous structure. The shape of each flexure region is

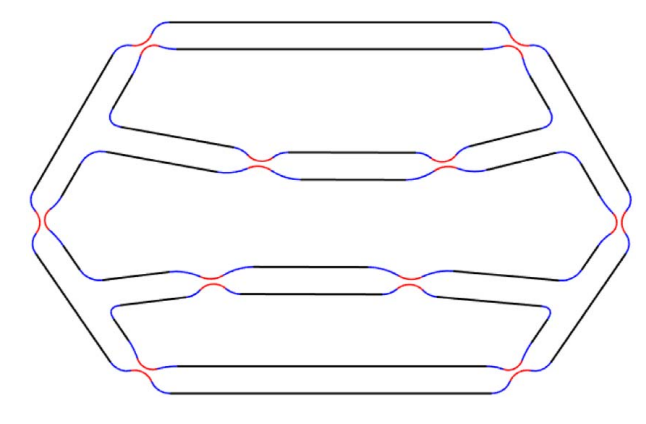


Fig. 16 The final geometry of the continuum mechanism

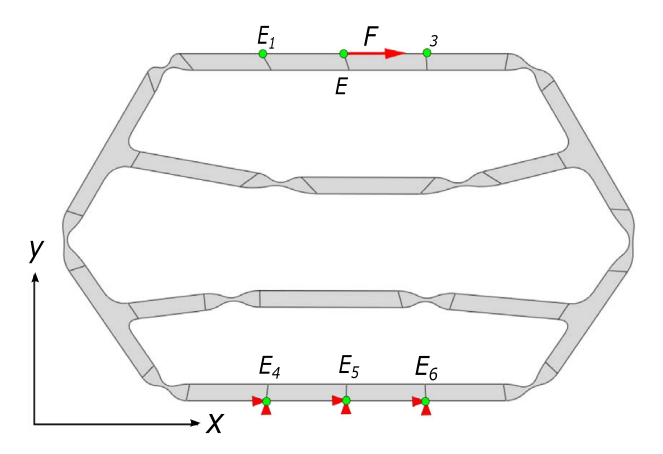


Fig. 17 The load and constraints of the FEM model

Table 2 The results of the FEM simulation we select with the material of Nylon-6

Nylon-6					
F (N)	Output stroke (mm)	Path deviation (μm)	Orientation deviation (milliradian)		
5.8	37.4	3.7	4.1		

Table 3 The results of the three parameters of each joint of the compliant eight-bar linkage

$t_k$	Length (mm)	$l_k$	Length (mm)	$d_k$	Length (mm)
$t_1$	0.76	$l_1$	9.20	$d_1$	5.54
$t_2$	1.35	$l_2$	8.95	$d_2$	10.98
$t_3$	0.87	$\bar{l_3}$	16.08	$\overline{d_3}$	10.79
$t_4$	0.87	$l_4$	13.94	$d_4$	6.66
$t_5$	1.24	$l_5$	15.11	$d_5$	11.30
$t_6$	0.96	$l_6$	15.79	$d_6$	8.07
$t_7$	1.01	$l_7$	10.64	$d_7$	11.25
$t_8$	0.79	$l_8$	6.99	$d_8$	6.82
t <sub>9</sub>	1.14	$l_9$	14.38	$d_9$	6.53
$t_{10}$	1.24	$l_{10}$	10.58	$d_{10}$	10.31

controlled by the three parameters, the initial values of these parameters are specified by the designer. With the different parameter values of the flexure regions, the output stroke and motion accuracy of the continuum mechanism are different when the mechanism is deformed. In order to distribute the stress uniformly to obtain an effective continuum mechanism with a larger output stroke and smaller deviation, we use FEA to identify a set of the parameter values within its ranges.

Here, ABAQUS software is applied to finite element analysis. As shown in Fig. 17, the boundary conditions of FEA are that nodes  $E_4$ ,  $E_5$ , and  $E_6$  which are on the basis are fixed on the ground, and a given force F is applied to the direction of the x-axis at the location of the node  $E_2$ . Here, the maximum displacement of node  $E_2$  in the direction of the x-axis is defined as the output stroke for the rectilinear movement, the maximum displacement of node  $E_2$  in the direction of y-axis is defined as path deviation of the rectilinear movement, and the maximum angle between line  $E_1E_3$  and x-axis is defined as the orientation deviation. In addition, the output stroke is denoted by  $x_{\rm max}$ , the path deviation is denoted by  $y_{\rm max}$ , and the orientation deviation is denoted by  $\theta_{\rm max}$ .

We select randomly multiple sets of these parameters values for iterative calculation, and identify a good one. The selection method is that using the rand(·) function in MATLAB software to generate

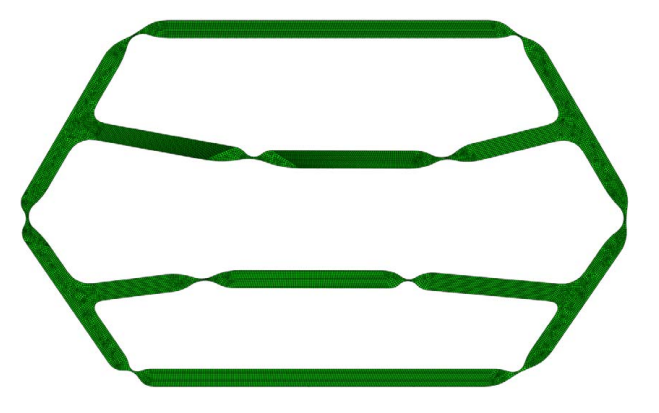


Fig. 18 The initial configuration of the continuum mechanism

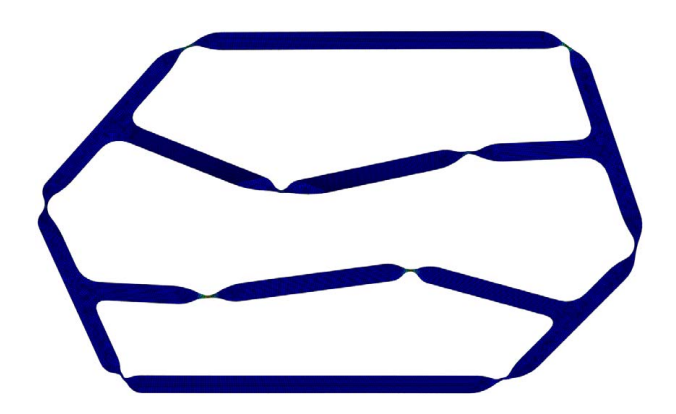


Fig. 19 The deformation configuration of the continuum mechanism

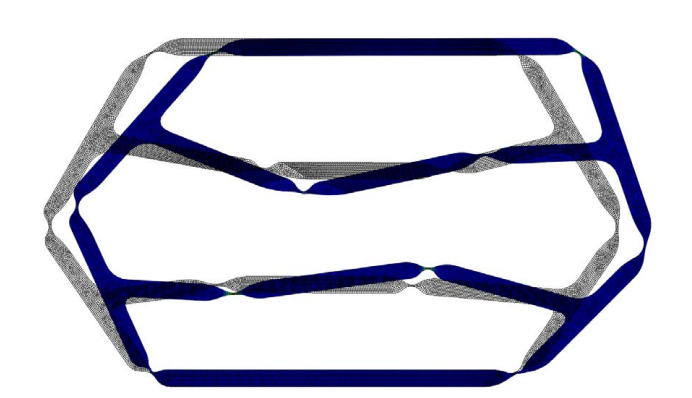


Fig. 20 The deformation configuration overlaps the initial configuration to demonstrate that the end-effector has the rectilinear movement

random number for each parameter within its range. So, the values of  $t_k$ ,  $l_k$ , and  $d_k$  for each iteration can be given by

$$t_{k} = (t_{k})_{\min} + [(t_{k})_{\max} - (t_{k})_{\min}] \times \text{rand}(0 \sim 1)$$

$$l_{k} = (l_{k})_{\min} + [(l_{k})_{\max} - (l_{k})_{\min}] \times \text{rand}(0 \sim 1)$$

$$d_{k} = (d_{k})_{\min} + [(d_{k})_{\max} - (d_{k})_{\min}] \times \text{rand}(0 \sim 1)$$

$$k = 1, \dots, 10.$$
(14)

**6.1 An Numerical Example.** Here, an numerical example is demonstrated to identify a good set of parameters. Let  $(t_k)_{\min} = 0.5 \text{ mm}$ ,  $(t_k)_{\max} = 1.5 \text{ mm}$ , h = 10 mm, and F = 5.8 N, and the thickness of the monolithic structure is 16 mm. The material is Nylon-6 with linear elastic material behavior and the following properties:

Table 4 Different scaling ratio performance with Nylon-6

Nylon-6							
Scaling ratio	F (N)	Output stroke (mm)	Path deviation (µm)	Orientation deviation (milliradian)			
1.3	8.7	46.9	8.3	10.3			
1	5.8	37.4	3.7	4.1			
0.6	2.0	21.5	3.3	3.2			
0.3	0.55	11.8	2.3	3.2			

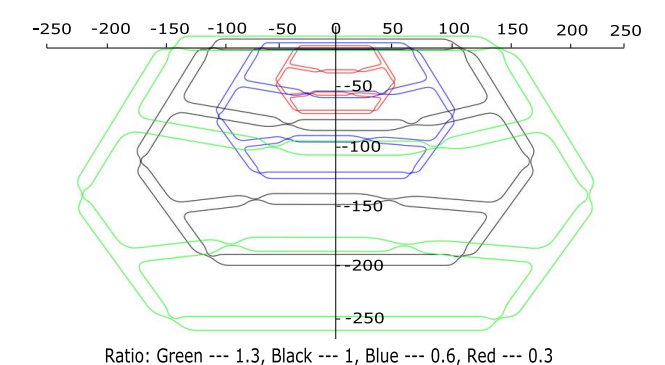


Fig. 21 The continuum mechanisms with different scaling ratios

Young's Modulus  $E_1 = 3\,450$  MPa, Poisson's ratio  $\mu_1 = 0.4$ , and yield strength  $\sigma_1 = 70$  MPa. The objectives are to obtain a large output stroke, small path deviation, and small orientation deviation linkage within the elastic deformation; thus, we have a criterion with a weight function and a constraint that is the maximum Von

Mises stress of the linkage is less than the material Yield strength during the deformation to select the effective mechanism,

min: 
$$f = \lambda_1 \frac{1}{x_{\text{max}}} + \lambda_2 y_{\text{max}} + \lambda_3 \theta_{\text{max}}$$
  
s.t.:  $S_{\text{max}} < \sigma_1$  (15)

where  $\lambda_1$ ,  $\lambda_2$ , and  $\lambda_3$  are weight factors and  $S_{max}$  denotes the maximum Von Mises stress of the continuum mechanism during the deformation.

Next, we organize 10,000 iterations of FEA calculation and identify an effective continuum mechanism for the rectilinear movement with 37.4 mm output stroke, 3.7  $\mu$ m path deviation and 4.1 milliradian orientation deviation, see Table 2. The final parameter values of each flexure region we selected are displayed in Table 3. The initial configuration and deformation configuration are shown in Figs. 18 and 19. And Fig. 20 shows the deformation configuration overlaps, the initial configuration to show that the end-effector of the continuum mechanism has the rectilinear movement.

**6.2** Geometric Scaling and Physical Prototype. This continuum mechanism for rectilinear movement can be scaled to any dimension for different application situations. The uniform geometric scaling approach which is a linear variation of all geometric lengths of the linkage is used to scale the mechanism. Here, the dimension of the mechanism obtained in Sec. 6.1 is defined as the basic dimension, namely, its scaling ratio is equal to 1 [27]. Then, we carry out FEA for the mechanisms whose scaling ratio are 1.3, 0.6, and 0.3, respectively, and their analysis results are shown in Table 4. The mechanisms with these different scaling ratios are shown in Fig. 21.

Based on these results, the output stroke changes in a linear variation with the scaling ratio, the path deviations and orientation deviations stay in the low micrometer range relative to the output stroke. In order to further verify our design, we manufactured a

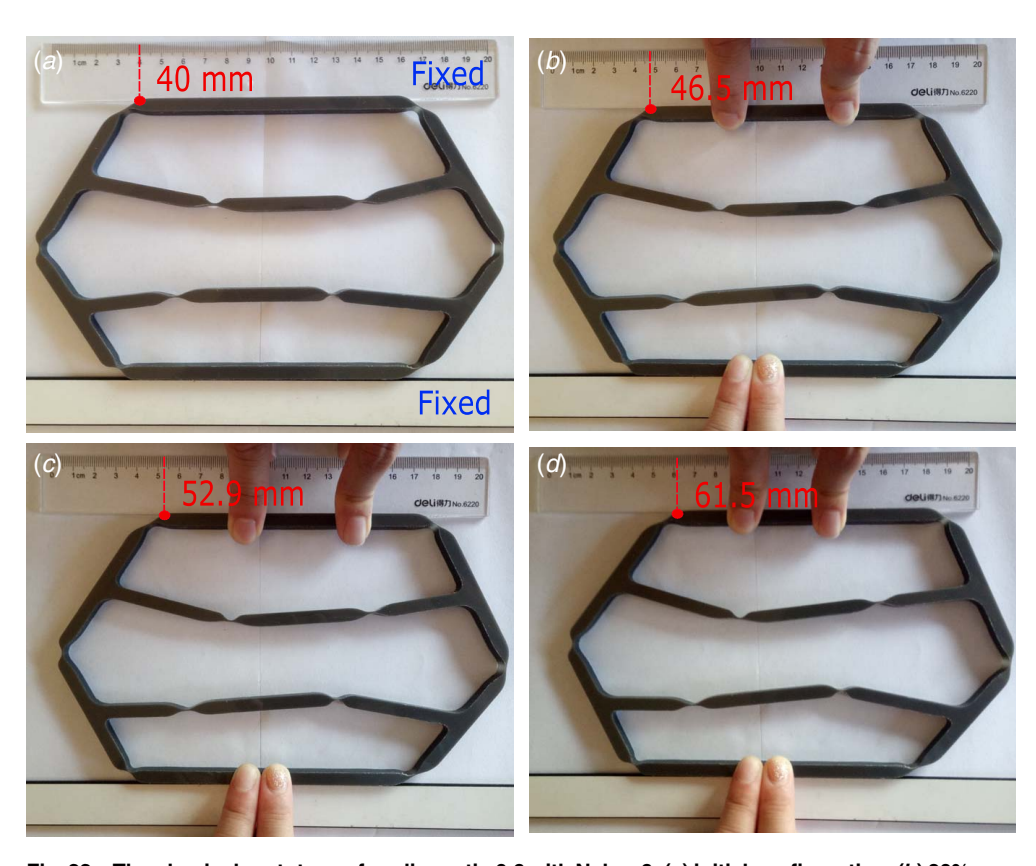


Fig. 22 The physical prototype pf scaling ratio 0.6 with Nylon-6: (a) initial configuration, (b) 30% progress of deformation, (c) 60% progress of deformation, and (d) 100% progress of deformation

physical prototype for the case of scaling ratio 0.6 with the material Nylon-6, which is shown in Fig. 22. When we use a horizontal force to drive the compliant eight-bar linkage, its end-effector can move 21.5 mm along a straight line.

# 7 Conclusions

This paper presents a design procedure that merges topological optimization for the design of compliant mechanisms with the kinematic synthesis of rigid link mechanisms. The primary strategy is to replace the phase of topological optimization that resolves the generic truss and beam structure using finite element analysis, with structures that are adapted to the required movement using the kinematic synthesis of rigid link mechanisms. The elements of the resulting model structure are dimensioned to provide the required force-deflection relationship. Special regions of deformation are introduced to coincide with the joints of the kinematic model. They are parameterized to provide a convenient way to iterate the continuous structure to obtain the desired movement and stress distribution in the continuum mechanism.

As an example, we use kinematic synthesis to compute the dimensions of an eight-bar rigid link mechanism that moves its workspace along a rectilinear path without link overlap. This mechanism is used to define the model structure for the design of a continuum linkage. The result is a continuum mechanism that provides the same movement as the original linkage. A physical model was constructed using Nylon-6 that was 120 mm in height and provided rectilinear movement over 21.5 mm with a deviation that was not perceptible.

### Acknowledgment

The authors gratefully acknowledge the support of the National Science Foundation under Grant No. 1636017. We also acknowledge the assistance of colleagues at the University of California, Irvine, Prof. Edwin A. Peraza Hernandez and Woo Rib Suh with the formulation of the FEA model, and Yujia Liu with the manufacture of the Nylon-6 physical model. Xueao Liu also acknowledges Hongyu Wu for many helpful discussions.

# **Data Availability Statement**

The datasets generated and supporting the findings of this article are obtainable from the corresponding author upon reasonable request. The authors attest that all data for this study are included in the paper.

# References

- [1] Hu, X., Chen, A., Luo, Y., Zhang, C., and Zhang, E., 2018, "Steerable Catheters for Minimally Invasive Surgery: a Review and Future Directions," Comput. Assisted Surg., 23(1), pp. 21–41.
- [2] Yamaguchi, T., Ambe, Y., Ando, H., Konyo, M., Tadakuma, K., Maruyama, S., and Tadokoro, S., 2019, "A Mechanical Approach to Suppress the Oscillation of a Long Continuum Robot Flying With Water Jets," IEEE Rob. Autom. Lett., 4(4), pp. 4346–4353
- [3] Greer, J. D., Morimoto, T. K., Okamura, A. M., and Hawkes, E. W., 2019, "A Soft, Steerable Continuum Robot that Grows via Tip Extension," Soft Rob., 6(1), pp. 95–108.
- [4] Howell, L. L., 2001, Compliant Mechanisms, Wiley-Interscience, New York.
- [5] Kota, S., Li, J., Rodgers, S. M., and Sniegowski, J., 2001, "Design of Compliant Mechanisms: Applications to MEMS," Analog Integrated Circuits Signal Process., 29(1–2), pp. 7–15.

- [6] Suh, W. R., McCarthy, J. M., and Peraza-Hernandez, E. A., 2019, "Efficient Development of Continuum/Compliant Planar Linkage Mechanisms," Proceedings of the ASME 2019 International Design Engineering Technical Conferences and Computers and Information in Engineering Conference, Volume 5A: 43rd Mechanisms and Robotics Conference, Anaheim, CA, Aug. 18–21, ASME, p. V05AT07A003.
- [7] Cao, L., Dolovich, A. T., Schwab, A. L., Herder, J. L., and Zhang, W., 2015, "Toward a Unified Design Approach for Both Compliant Mechanisms and Rigid-Body Mechanisms: Module Optimization," ASME J. Mech. Des., 137(12), p. 122301.
- [8] Valentini, P. P., and Pennestri, E., 2018, "Compliant Four-Bar Linkage Synthesis With Second-Order Flexure Hinge Approximation," Mech. Mach. Theory, 128, pp. 225–233.
- [9] Saxena, A., and Ananthasuresh, G. K., 2001, "Topology Optimiationa of Compliant Mechanisms With Strength Considerations," Mech. Struct. Mach., 29(2), pp. 199–221.
- [10] Cao, L., Dolovich, A., and Zhang, W. J., 2013, "On Understanding of Design Problem Formulation for Compliant Mechanisms Through Topology Optimization," Mech. Sci., 4(2), pp. 357–369.
- [11] McCarthy, J. M., and Soh, G. S., 2011, Geometric Design of Linkages, Springer, New York.
- [12] Sonawale, K. H., and McCarthy, J. M., 2015, "Design of Eight-Bar Linkages With an Application to Rectilinear Motion," Proceedings of the ASME 2015 International Design Engineering Technical Conferences and Computers and Information in Engineering Conference. Volume 5B: 39th Mechanisms and Robotics Conference, Boston, MA, Aug. 2–5, ASME, p. V05BT08A084.
- [13] Sonawale, K. H., and McCarthy, J. M., 2016, "A Design System for Eight-Bar Linkages as Constrained 4R Serial Chains," J. Mech. Robot., 8(1), p. 011016.
- [14] Su, H. J., 2009, "A Pseudorigid-Body 3R Model for Determining Large Deflection of Cantilever Beams Subject to Tip Loads," J. Mech. Robot., 1(2), p. 021008.
- [15] Su, H. J., and McCarthy, J. M., 2007, "Synthesis of Bistable Compliant Four-Bar Mechanisms Using Polynomial Homotopy," ASME J. Mech. Des., 129(10), pp. 1094–1098
- [16] Lobontiu, N., 2002, Compliant Mechanisms: Design of Flexure Hinges, CRC Press, Boca Raton, FL.
- [17] LinLinß, S., and Milojevic, A., 2012, "Model-Based Design of Flexure Hinges for Rectilinear Guiding with Compliant Mechanisms in Precision Systems," Mechanismentechnik in Ilmenau, Budapest und Niš. Ilmenau: Universitätsverlag Ilmenau, pp. 13–24.
- [18] Shi, Q., Wang, S., Qiu, A., Xu, Y., and Ji, X., 2006, "Design Principle of Suspension of MEMS Gyroscope," 2006 1st IEEE International Conference on Nano/Micro Engineered and Molecular Systems, Zhuhai, China, Jan. 18–21,
- [19] Mackay, A. B., Smith, D. G., Magleby, S. P., Jensen, B. D., and Howell, L. L., 2012, "Metrics for Evaluation and Design of Large-Displacement Linear-Motion Compliant Mechanisms," ASME J. Mech. Des., 134(1), p. 011008.
- [20] Hao, G., Kong, X., and He, X., 2014, "A Planar Reconfigurable Linear Rigid-Body Motion Linkage With Two Operation Modes," J. Mech. Eng. Sci., 228(16), pp. 2985–2991.
- [21] Liu, Y., and McCarthy, J. M., 2015, "Flexure Design for Eight-Bar Rectilinear Motion Mechanism," Proceedings of the ASME 2015 International Design Engineering Technical Conferences and Computers and Information in Engineering Conference. Volume 5A: 39th Mechanisms and Robotics Conference, Boston, MA, Aug. 2–5., ASME, p. V05AT08A025.
- [22] Kempe, A., 1877, How to Draw a Straight Line: A Lecture on Linkages (Cornell University Library Historical Math Monographs), Macmillan and Company.
- [23] Howell, L. L., and Midha, A., 1994, "A Method for the Design of Compliant Mechanisms With Small-Length Flexural Pivots," ASME J. Mech. Des., 116(1), pp. 280–290.
- [24] Xu, Q., 2017, Design and Implementation of Large-Range Compliant Micropositioning Systems, John Wiley Sons, Singapore.
- [25] Parrish, B. E., and McCarthy, J. M., 2013, "Use of the Jacobian to Verify Smooth Movement in Watt I and Stephenson I Six-Bar Linkages," Proceedings of the ASME 2013 International Design Engineering Technical Conferences and Computers and Information in Engineering Conference. Volume 6A: 37th Mechanisms and Robotics Conference, Portland, OR, Aug. 4–7, ASME, p. V06AT07A057.
- [26] Sonawale, K. H., and McCarthy, J. M., 2014, "Synthesis of Useful Eight-Bar Linkages as Constrained 6R Loops," Proceedings of the ASME 2014 International Design Engineering Technical Conferences and Computers and Information in Engineering Conference. Volume 5A: 38th Mechanisms and Robotics Conference, Buffalo, NY, Aug. 17–20, ASME, p. V05AT08A076.
  [27] Linß, S., Henning, S., and Zentner, L., 2019, "Modeling and Design of Flexure
- [27] Linß, S., Henning, S., and Zentner, L., 2019, "Modeling and Design of Flexure Hinge-Based Compliant Mechanisms," *Kinematics – Analysis and Applications*, J. Mizrahi, ed., IntechOpen.